Carbon 113 (2017) 243–251

Contents lists available at ScienceDirect

Carbon

journal homepage: www.elsevier.com/locate/carbon

# Hollow carbon spheres trigger inflammasome-dependent IL-1β secretion in macrophages

Fernando T. Andón [a, b, c, 1], Sourav P. Mukherjee [a, 1], Isabel Gessner [d], Laura Wortmann [d], Lisong Xiao [d], Kjell Hultenby [e], Anna A. Shvedova [f, g], Sanjay Mathur [d], Bengt Fadeel [a, *]

[a] Division of Molecular Toxicology, Institute of Environmental Medicine, Karolinska Institutet, 17177, Stockholm, Sweden
[b] Laboratory of Cellular Immunology, Humanitas Clinical and Research Institute, 20089, Rozzano-Milano, Italy
[c] Pharmacy & Pharmaceutical Technology Department, Centre of Research in Molecular Medicine and Chronic Diseases, University of Santiago de Compostela, 15705, Santiago de Compostela, Spain
[d] Inorganic and Materials Chemistry, University of Cologne, 50939, Cologne, Germany
[e] Clinical Research Center, Department of Laboratory Medicine, Karolinska Institutet, Karolinska University Hospital Huddinge, 14185, Stockholm, Sweden
[f] Health Effects Laboratory Division, National Institute for Occupational Safety and Health, Morgantown, WV, 26505, United States
[g] Department Pharmacology & Physiology, West Virginia University, Morgantown, WV, 26505, United States

ARTICLE INFO

*Article history:*
Received 12 October 2016
Received in revised form
16 November 2016
Accepted 18 November 2016
Available online 22 November 2016

ABSTRACT

It is disputed whether inflammasome activation leading to secretion of pro-inflammatory interleukin (IL)-1β in macrophages transpires independently of cell death or whether the two processes are linked. Here, we synthesized hollow carbon spheres (HCS) and investigated their effects on primary human monocyte-derived macrophages (HMDM); short (500 nm) non-functionalized single-walled carbon nanotubes (SWCNT) were included for comparison. HCS (250 nm) were readily taken up by HMDM and induced ROS production, but did not trigger a loss of cell viability. However, a dose- and time-dependent release of IL-1β was detected in lipopolysaccharide (LPS)-primed macrophages upon exposure to HCS, while SWCNT-induced secretion of IL-1β was less pronounced. HCS-triggered IL-1β secretion was cathepsin B- and caspase-1-dependent, and was accompanied by a reduction in intracellular $K^+$. Furthermore, cytokine secretion was reduced following treatment with the antioxidant, *N*-acetylcysteine, and cytochalasin D, an inhibitor of actin polymerization. HCS also triggered IL-1β release in LPS-primed THP.1 cells, but not in THP.1 cells with silencing of ASC, NLRP3, or caspase-1 expression, providing evidence that IL-1β was elicited through NLRP3 inflammasome activation. These studies shed light on the effects of HCS on primary macrophages, and show that spherical carbon-based nanoparticles are potent inflammasome activators.



## 1. Introduction

Carbon-based nanomaterials (CBMs) hold significant promise in the fields of medicine and engineering due to their intrinsic physicochemical properties [1,2]. The most well-studied CBMs to date from a biological perspective are single- and multi-walled carbon nanotubes (CNTs), and two-dimensional (2-D) graphene oxide (GO), both presenting excellent and attractive properties, such as high chemical stability, strong mechanical integrity, along with desirable electric and thermal properties [2]. However, CBMs have also been shown to exert toxicological effects, both *in vitro* and *in vivo* [3]. Moreover, novel CBMs, such as hollow carbon spheres (HCS), have recently received considerable attention for their use in energy storage devices (*i.e.*, supercapacitors, lithium-ion batteries, fuel cells and hydrogen storage devices), owing to their unique three-dimensional structure and functional behavior, such as very high specific surface area, low specific density, large controllable inner pore volume, and good mechanical strength [4–6]. To date, few studies have addressed the potential toxicity of HCS.

*Abbreviations:* ASC, apoptosis-associated speck-like protein; CBMs, carbon-based nanomaterials; HCS, hollow carbon spheres; HMDM, human monocyte-derived macrophages; LAL, limulus amoebocyte lysate; LPS, lipopolysaccharide; NAC, *N*-acetyl-cysteine; NLRP3, NLR (nucleotide-binding domain and leucine-rich repeat containing) family pyrin domain containing 3 (also known as NALP3; for NACHT, LRR and PYD domain-containing protein 3).

* Corresponding author.
*E-mail address:* Bengt.Fadeel@ki.se (B. Fadeel).

[1] These authors contributed equally to this work.

http://dx.doi.org/10.1016/j.carbon.2016.11.049
0008-6223/

Cell death is typically dichotomized into apoptosis, a programmed and anti-inflammatory mode of cell death, and necrosis, which is commonly viewed as accidental and pro-inflammatory [7]. There are examples of the induction both of apoptosis and necrosis by SWCNT and by GO [8–12], although the molecular mechanisms in most cases remain to be characterized. Besides, additional forms of cell death commonly related with the induction of pro-inflammatory responses, such as pyroptosis, a caspase-1-dependent form of cell death, have also been described [13], but there are few studies on the possible relevance of these modes of cell death for nanomaterial-induced toxicity. On the other hand, an emerging body of literature demonstrates that engineered nanomaterials, including multi-walled CNTs [14–16] and small, spherical carbon nano-onions [17], are able to activate the inflammasome complex in phagocytic cells (macrophages) with subsequent secretion of pro-inflammatory interleukin (IL)-1β [18]. This may be of particular relevance for our understanding of the health risks of inhaled particles (see Ref. [19] for a recent review). However, the link between inflammasome activation and cytotoxicity of nanomaterials, or other exogenous agents, is not well understood, although recent studies have pointed to a role for lysosomes both for activation of the NLRP3 inflammasome and for certain forms of programmed cell death induced by nanomaterials [7]. Overall, understanding the cellular signaling pathways that are engaged by nanoparticles may lead to more refined approaches for the assessment and mitigation of adverse effects of such materials. Here, we performed detailed studies of the impact of hollow carbon spheres (HCS) on primary human monocyte-derived macrophages (HMDM). Our results clearly show that HCS are potent activators of the NLRP3 inflammasome, without any loss of macrophage cell viability.

## 2. Experimental

### 2.1. Reagents

The cell permeable inhibitors, zVAD-fmk, WEHD-fmk, and CA-047-Me, as well as *N*-acetyl-L-cysteine (NAC), lipopolysaccharide (LPS), and nigericin were from Sigma Aldrich (St. Louis, MO). ZnO nanoparticles (ZincoxTM 10) were from IBU-Tec Advanced Materials AG (Weimar, Germany), and material characterization has been reported previously by us [20]. Fetal bovine serum (FBS) and RPMI-1640 cell culture medium were from Invitrogen (Paisley, UK).

### 2.2. Nanomaterial synthesis and characterization

SWCNTs (obtained from CNI, Inc., Houston, TX) were produced by the high pressure CO disproportionation process (HiPco) technique [21]. CO was employed in a continuous-flow gas phase as the carbon feedstock and $Fe(CO)_5$ as the iron-containing catalyst precursor, and the SWCNTs were purified by acid treatment to remove metal contaminates. Chemical analysis of trace metal (iron) revealed that the SWCNTs comprised 0.23 wt % iron. Surface area was determined by Brunauer, Emmett, and Teller (BET) analysis, and diameter and length were measured by transmission electron microscopy (TEM), as described previously [21]. The mean length, diameter and surface area of SWCNTs were 500 nm, 1–4 nm, and 1040 $m^2/g$, respectively. HCS were prepared by a template-assisted solvothermal synthesis following a previously published procedure [22]. $SiO_2$ particles, used as templates, were prepared using tetraethyleorthosilicate (TEOS) (98%, Sigma-Aldrich, Germany) as precursor following a modified Stöber-method [23]. In a typical synthesis, $SiO_2$ particles were coated with glucose followed by etching of the $SiO_2$ core. The 40 mg of as-prepared $SiO_2$ particles were dispersed in 1 ml ethanol and mixed with 19 ml of a 0.5 M D-glucose (D(+)-Glucose, Acros Organics, Germany) solution. The mixture was sonicated for 10 min and then filled into a Teflon lined tube ($V_{max}$ = 50 ml), which was transferred into a steel autoclave and heated at 180 °C for 10 h. The resulting brown particles were washed five times with water via centrifugation and redispersion. Thereafter, particles were dried in a vacuum oven at 60 °C for 6 h and subsequently the glucose coating was graphitized for 3 h at 500 °C under reducing atmosphere. The silica template was finally removed by stirring the particles for 24 h in 10 ml of 1 M hydrofluoric acid (HF) (48%, Sigma-Aldrich). HCS were washed five times with water and ethanol before characterization and further use. The size distribution of HCS was investigated by TEM and dynamic light scattering (DLS). The morphology of HCS was assessed by scanning electron microscopy (SEM) using a FEI Quanta 50 FEG Series microscope. TEM was performed on a ZEISS Leo912 microscope operated at an acceleration voltage of 120 kV. 10 μL of a diluted HCS dispersion was dropped on a carbon-covered standard TEM grid (QUANTIFOIL Multi A) and dried under air. Electrophoretic mobility (μ) was measured by Malvern Zetasizer Nano ZS at 633 nm after dilution of samples with water or in cell culture medium supplemented with 10% FBS. Default instrument settings and automatic analysis were used for all measurements, where the μ was converted automatically by the equipment software to zeta potential (ζ) values as it is directly related to the zeta potential by Henry's equation. All average values for samples prepared were based on triplicate measurements. The chemical composition of HCS was studied by X-ray photoelectron spectroscopy (XPS) and recorded using a Surface Science Instruments ESCA M-Probe XPS spectrometer with a monochromatic Al K-α source of 1486.68 eV. The survey XPS spectra were acquired with pass energy (PE) of 158.9 eV, 0.5 eV step size, 125 ms dwell time and averaged over 7 scans. The high resolution C1s XPS spectra were acquired with PE of 22.9 eV, 0.05 eV step size, 175 ms dwell time and averaged over 25 scans. Spectra of the insulating samples were charge corrected by shifting all peaks to the adventitious carbon C1s spectral component binding energy set to 284.8 eV. CasaXPS software was used to process the spectra. Finally, Fourier Transform Infrared (FT-IR) spectra of HCS were recorded between 400 and 4000 $cm^{-1}$ using a Perkin Elmer FT spectrometer.

### 2.3. Macrophage isolation and culture

Peripheral blood mononuclear cells (PBMC) were prepared from buffy coats obtained from healthy blood donors (Karolinska University Hospital, Stockholm, Sweden) by density gradient centrifugation using Lymphoprep (Axis-Shield, Oslo, Norway) as described before [24]. Briefly, monocytes were positively selected for based on CD14 expression using CD14 MicroBeads (Miltenyi Biotec, Bergisch Gladbach, Germany). To obtain human monocyte-derived macrophages (HMDM), $CD14^+$monocytes were cultured in RPMI-1640 medium supplemented with 2 mM L-glutamine, 100 IU/ml penicillin, 100 mg/ml streptomycin, 10% heat-inactivated FBS, with 50 ng/ml recombinant macrophage colony-stimulating factor (M-CSF) (Novakemi, Handen, Sweden) for 3 days. For priming experiments, HMDM were first incubated with 100 ng/ml of LPS for 1 h prior to exposure, according to established procedures [14].

### 2.4. THP.1 knockdown cell lines

THP.1 is a human monocytic cell line that naturally expresses many pattern recognition receptors, including Toll-like receptors

(TLRs). In this study we employed four different THP.1 cell lines (*i.e.*, Null-1, defASC, defNLRP3 and defCaspase-1) obtained from InvivoGen (France). The THP.1 null (positive control) and knockdown cells [25] were cultured according to the manufacturers' instructions. After sub-culturing the cells thrice in the recommended growth medium, they were seeded in 96-well plates at a density of $10^5$ cells/well. After 24 h of seeding, one set of cells were primed with 100 ng/ml lipopolysaccharide (LPS) for 2 h and the other set were kept un-primed. Then, the cells were exposed to 30 μg/ml of HCS in 10% FBS-supplemented growth medium for 24 h. Following this period, cell culture media were collected and IL-1β content was measured using a standard ELISA as detailed below in Section 2.11.

### 2.5. Endotoxin assessment

Endotoxin content was assessed using the chromogenic Limulus Amebocyte Lysate (LAL) assay (Charles River Endosafe, Charleston, SC). The endotoxin content in HCS and SWCNT samples was found to be below FDA-mandated limits of acceptance (0.5 EU/ml) (data not shown).

### 2.6. Cell uptake of particles

To assess for cellular uptake and ultrastructural changes following exposure, HMDM were incubated with the indicated nanomaterials in cell culture medium supplemented with 10% FBS and then washed with PBS, trypsinated, and centrifuged at 2000 rpm for 3 min. Cells were then fixed in 2% glutaraldehyde in 0.1 M sodium cacodylate buffer containing 0.1 M sucrose and 3 mM $CaCl_2$, pH 7.4. Cells were washed in buffer and postfixed in 2% osmium tetroxide in 0.07 M sodium cacodylate buffer containing 1.5 mM $CaCl_2$, pH 7.4, at 4 °C for 2 h, dehydrated in ethanol followed by acetone, and embedded in LX-112 (Ladd, Burlington, VT). Sections were contrasted with uranyl acetate followed by lead citrate and were examined in a Tecnai 12 Spirit Bio TWIN TEM (FEI Company, Eindhoven, The Netherlands) at 100 kV. Images were taken using a Veleta camera (Olympus Soft Imaging Solutions, GmbH, Münster, Germany).

### 2.7. Cell viability assessment

HMDM were exposed to nanomaterials in RPMI-1640 medium supplemented with 10% FBS and cell viability was assessed by using the Alamar Blue assay. Briefly, supernatants of HMDM exposed to particles for 24 h were removed and cells were washed three times with PBS. Then, AlamarBlue® reagent (ThermoFisher Scientific) diluted in RPMI medium (1:10) was added to each well and incubated for 2 h at 37 °C. Fluorescence was measured at 560 nm excitation and 590 nm emission wavelengths using a Tecan Infinite F200 plate reader. The metabolic activity of exposed cells was expressed by comparing their fluorescence with the untreated cells.

### 2.8. ROS measurements

Intracellular ROS levels were measured using the dichlorodihydrofluorescein diacetate (DCFH-DA) assay. Briefly, HMDM were seeded in black 96-well plates with transparent bottom at a density of $5 \times 10^4$ cells per well. After exposure, cells were washed with Hank's buffered salt solution (HBSS) and loaded with 20 μM DCFHDA in HBSS for 30 min at 37 °C. Thereafter, cells were washed with HBSS and fluorescence was recorded (excitation 485 nm, emission 535 nm) using a plate reader (Tecan Infinite F200) at 37 °C. Each experiment was repeated at least 3 times using cells from different donors (each sample in triplicate), and results were plotted as %ROS activity of macrophages incubated in medium alone, which was set at 100%.

### 2.9. Lysosomal activation

To assess for lysosomal activation with release of cathepsin B, we used the Magic Red™-cathepsin B substrate from Immunochemistry Technologies (Bloomington, MN). HMDM were exposed to HCS at 30 μg/ml concentration for the indicated time-points in 96-well plate or on 8-well chamber slides. Then, medium was removed and the cells were washed with warm (37 °C) PBS. The cells were then stained with the Magic Red™-cathepsin B substrate in PBS for 1 h at 37 °C in 5% $CO_2$. For 96-well plates, after the incubation time the cells were washed with PBS and the fluorescence of Magic Red™ was measured at excitation/emission of 540/590 nm (bandwidth Ex./Em. ± 24/20 nm) using a spectrophotometer (Infinite F200, Tecan, Männedorf, Switzerland, or Multiskan Ascent, Thermo Scientific). The fluorescent intensity measured is directly proportional with the amount of cathepsin-B released in the cytosol. The results are expressed as a percentage increase compare to the unexposed negative control cells. For 8-well chamber slides, the cells were washed with PBS and fixed in 4% paraformaldehyde for 20 min. Following washes with PBS, the cells were mounted with DAPI containing mounting solution (ProLong® Gold antifade reagent with DAPI, Life Technologies, Sweden) and visualized using a ZEISS LSM510META confocal microscope (Carl Zeiss, Oberkochen, Germany).

### 2.10. Intracellular potassium

HMDM were exposed for 24 h to HCS at 30 μg/ml and 100 μg/ml concentrations in 96-well plates. Nigericin (15 μM) was used as a positive control. Following exposure, medium was removed and the cells were washed with warm (37 °C) PBS. The cells were then stained with the potassium ($K^+$)-sensitive fluorophore, PBFI-AM (ThermoFisher Scientific) at 5 μM in PBS for 1 h at 37 °C in a 5% $CO_2$ incubator. Cells were then washed with PBS and fluorescence was measured at excitation/emission of 360/465 nm (bandwidth±35 nm) using a spectrophotometer (Infinite F200, Tecan, Männedorf, Switzerland, or Multiskan Ascent, Thermo Scientific). The fluorescent intensity is directly proportional to the intracellular K+. The results are expressed as a percentage decrease compared to the unexposed negative control cells.

### 2.11. Cytokine detection

Cell culture supernatants from HMDM exposed to nanomaterials were harvested and kept at −80 °C until analysis. Tumor necrosis factor (TNF)-α and IL-1β release were determined by ELISA (Mabtech, Nacka, Sweden) according to the manufacturer's instruction. Absorbance was measured at 405 nm using a Tecan Infinite F200 plate reader. Results are expressed as pg/ml of released cytokine, based on three independent experiments using cells from different donors.

### 2.12. Statistical analysis

All experiments were conducted in at least triplicate (three independent experiments). Statistical significance was tested with unpaired two-tailed Student *t* test or using one-way ANOVA with Tukey correction using GraphPad Prism version 5.02 for Windows (GraphPad Software, San Diego, CA). Data are reported as mean ± S.D. or S.E.M., as indicated in the figures.

## 3. Results and discussion

### 3.1. Synthesis and characterization of hollow carbon spheres

HCS are 3-D hollow carbon spheres consisting of a carbonized core and a polysaccharide coating bearing carbonyl-, alcohol- and carboxyl-groups present on the surface [26]. HCS, with low density and high surface-to-volume ratio, have attracted considerable attention as a consequence of their potential applications in catalyst supports, fuel cells, gas storage and separation, and lithium-ion batteries [27,28]. Templating approaches for fabrication of HCS are based on the carbonization of polymers followed by removal of the template. In the present study, we used inexpensive renewable carbohydrate precursors in combination with $SiO_2$ colloid templates [22], thus providing a simple, versatile and economical synthetic route which offers material property control in terms of surface chemistry, size and shell thickness. The synthesized HCS were subjected to rigorous physicochemical characterization. SEM and TEM analyses revealed that the synthesized HCS are monodispersed and uniformly spherical, thus retaining the morphology of the silica templates (Fig. 1a and b). The relative higher contrast of the shell with respect to the center zone confirms that the nanoparticles are hollow (Fig. 1b). TEM analysis showed an average outer diameter of 250 ± 30 nm and an average shell thickness of 65 ± 5 nm. The inner cavity of average 130 ± 20 nm is in accordance with the templates used. DLS measurements revealed a hydrodynamic diameter of 2283 ± 399 nm and a zeta potential of −38.61 mV in deionized $H_2O$, while the hydrodynamic diameter was found to be 336 ± 91 nm in cell culture medium supplemented with serum, suggesting a stabilization of the particles, with a zeta potential of −13.59 ± 3.38 mV (Table 1). SWCNTs produced by the HiPco technique and purified by acid treatment to remove metal contaminants were included in the present study. The chemical cutting procedure to obtain short (500 nm) SWCNTs was described previously [21].

Silica (amorphous and crystalline) is known to trigger inflammasome activation [29,30]. Therefore, prior to any biological testing, samples were treated with HF to remove residual silica scaffolds. XPS measurements indicated that the silica was completely removed after HF treatment (Fig. S1a) and small amounts of fluorine were detectable in the form of C—F bonds as seen in the high resolution C1s XPS measurements (Fig. S1b). While fluorination of carbon materials often results in semi-ionic or nearly-covalent C—F bonds, here, the high binding energy of 291.9 mV can be correlated to covalent C—F bonds of $CF_2$ or $CF_3$ [31], which also explains the hydrophobic nature of HCS. The presence of C—F bonds was further supported by FT-IR spectrometric analysis after graphitization of HCS (Fig. S2). Besides the presence of C=C and C=O bands at 1680–1620 $cm^{-1}$, 675–900 $cm^{-1}$ and 1750 $cm^{-1}$, respectively, bands which are characteristic for covalent C—F bonds between 1210 and 1250 $cm^{-1}$ were revealed. The broad band between 1000 and 1500 $cm^{-1}$ probably also includes C—O—C and C—OH vibrations (Fig. S2).

### 3.2. Macrophage internalization of hollow carbon spheres

An important issue when assessing the interaction of nanomaterials with immune-competent cells is the potential contamination of the samples with bacterial endotoxin or lipopolysaccharide (LPS), a component of all Gram-negative bacteria and one of the most potent activators of innate immunity. Even small amounts of LPS can trigger the production of pro-inflammatory mediators such as TNF-α [32], and may explain the maturation of antigen-presenting cells induced by LPS-contaminated nanoparticles [33]. Therefore, we tested our particles for endotoxin content using the conventional, chromogenic LAL assay, and we performed a macrophage activation test based on detection of TNF-α production by HMDM upon exposure to the test material (Mukherjee et al., in press). LPS (100 ng/ml) was included as a positive control. Both CBMs were found to be endotoxin-free by these methods (data not shown).

TEM imaging was performed to assess whether SWCNT and HCS (10 μg/ml) are taken up by primary macrophages. Indeed, intracellular localization of HCS was observed at 2 h and particles remained in the cells at 12 h with no obvious morphological signs of cytotoxicity (Fig. 2c). Individual SWCNT are difficult to visualize by TEM; however, large agglomerates of SWCNT present in cell culture medium dispersions were readily identified in close approximation to macrophages after 2 h and internalized bundles of SWCNTs were seen within intracellular vacuoles/vesicles at 24 h (Fig. S3c). Thus, both CBMs could be internalized by HMDM.

### 3.3. No cell death in macrophages exposed to hollow carbon spheres

Next, we assessed the cell viability of HMDM exposed to HSC using the Alamar Blue assay. Alamar Blue is a sensitive oxidation-reduction indicator that both fluoresces and undergoes colorimetric change in response to reduction by living cells. The reduction of Alamar Blue is believed to be mediated by mitochondrial enzymes although cytosolic and microsomal enzymes probably also contribute [34]. The assay was found to be more sensitive than

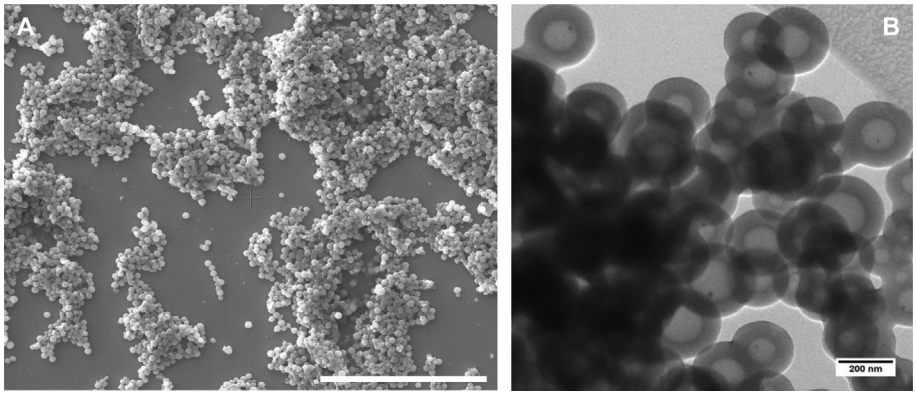


**Fig. 1.** Hollow carbon spheres (HCS). (A) SEM (scale bar: 20 μm) and (B) TEM analysis (scale bar: 200 nm) showing morphology and size. Refer to Table 1 for a summary of the particle properties.

**Table 1**
Physicochemical characterization of HCS.

| Dispersant | Particle size (nm) | Shell thickness (nm) | Hydrodynamic size (nm) | Zeta potential (mV) |
|---|---|---|---|---|
| Deionized water, $dH_2O$ | 250 ± 30 | 65 ± 5 | 2283 ± 399 | −38.61 ± 1.62 |
| RPMI-1640 + 10% FBS | N/A | N/A | 336 ± 91 | −13.59 ± 3.38 |

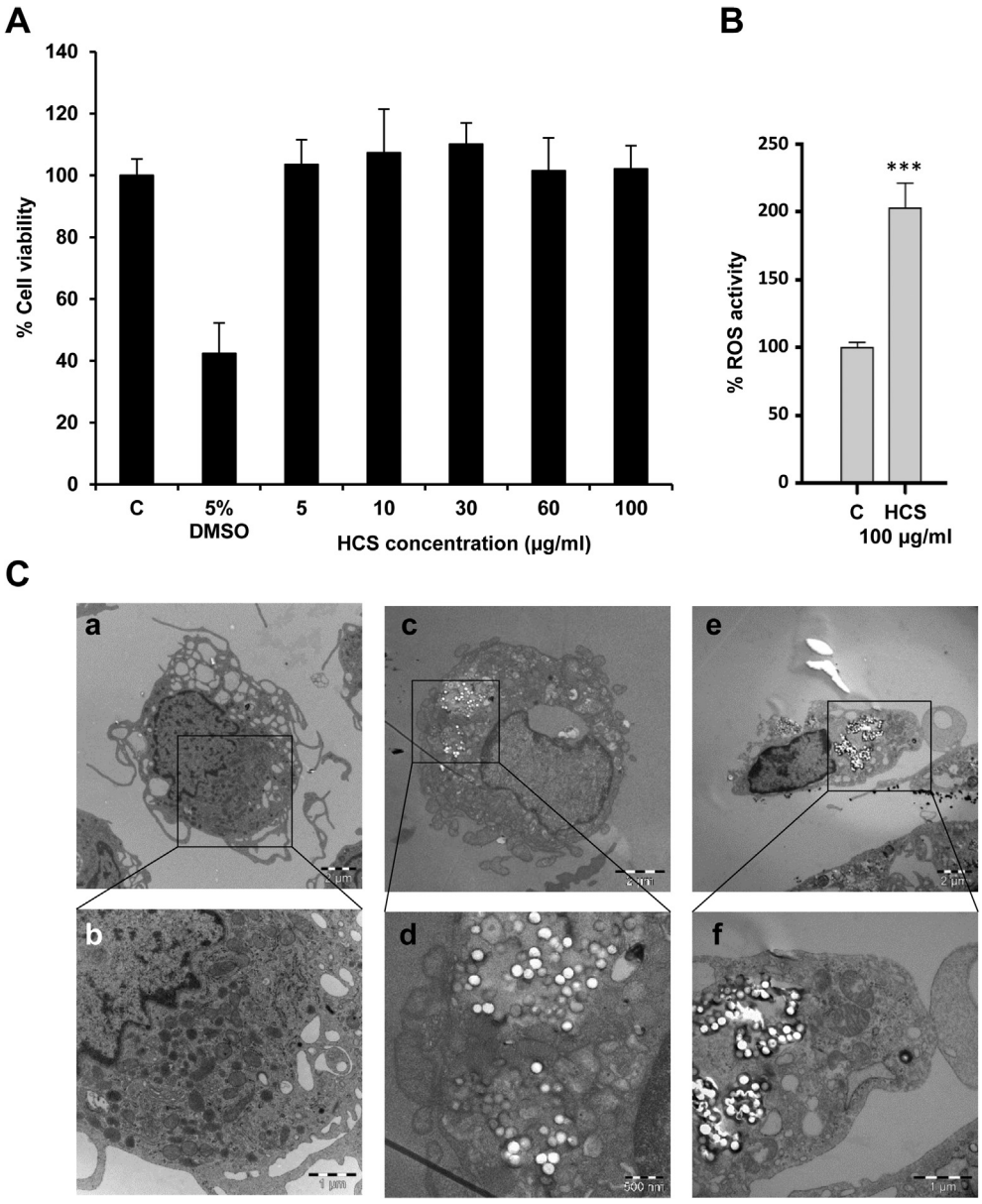


**Fig. 2.** Interaction of HCS with primary human monocyte-derived macrophages (HMDM). (A) Cell viability assessment using the Alamar Blue assay. HMDM were primed with lipopolysaccharide (LPS) for 2 h prior to exposure to HCS. DMSO (5%) was used a positive control for cell death. (B) ROS production in HMDM exposed to HCS (100 μg/ml) for 24 h, as determined using the DCFH-DA assay. Results in (A) and (B) are shown as mean ± S.D. of three independent experiments using cells from different human blood donors. ***$p < 0.001$. (C) TEM imaging of HMDM incubated in medium alone (panel a, b), or exposed to HCS (10 μg/ml) for 2 h (panel c, d), or 12 h (panel e, f). Scale bars: 2 μm (a, c, e), or 1 μm (b, f), or 500 nm (d).

the MTT assay [34]. It is important to note that some classical toxicology assays may not be suitable for assessing nanoparticle cytotoxity due to interference with the assays; this is true not least for some CBMs, such as CNTs [35]. However, HCS did not interfere with Alamar Blue detection (cell-free) (data not shown). As seen in Fig. 2a, there was no loss of cell viability in HMDM exposed to HCS at concentrations ranging from 5 to 100 μg/ml. DMSO (5%) was used as a positive control. The cells were LPS-primed prior to exposure to HCS in order to allow for a comparison with subsequent studies of cytokine secretion using LPS-primed HMDM (see below).

We also found that HCS (100 μg/ml) triggered cellular ROS production (Fig. 2b). Oxidative stress is frequently implicated in cell death induction by nanoparticles, although ROS production *per se* does not necessarily imply that a cell is undergoing cell death;

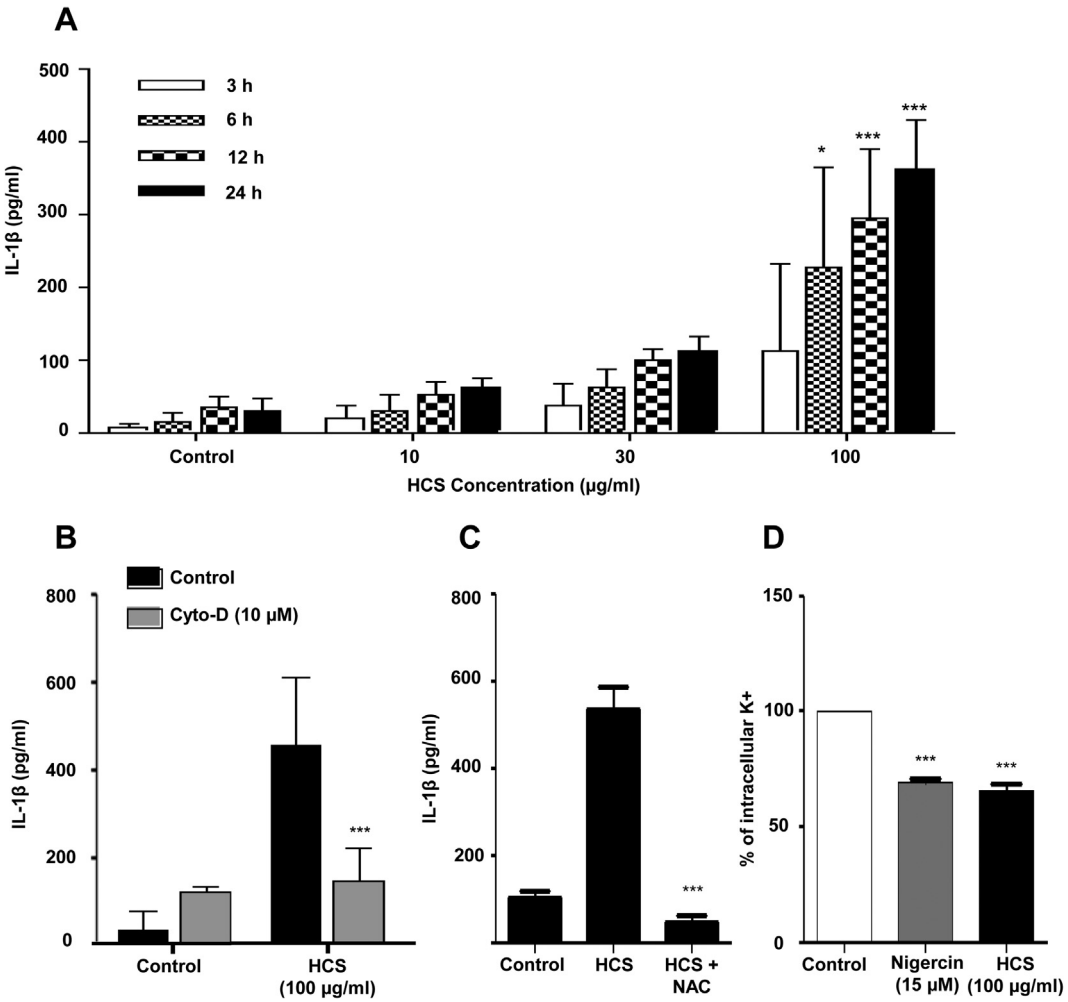


**Fig. 3.** HCS-triggered IL-1β secretion: exploring the molecular pathway. (A) LPS-primed HMDM were exposed to HCS at the indicated concentrations and time-points, and IL-1β content (pg/ml) in cell culture supernatants was assessed using a specific ELISA. (B) IL-1β secretion in LPS-primed HMDM pretreated or not with cytochalasin D (10 μM) followed by exposure for 24 h to HCS (100 μg/ml). (C) IL-1β secretion in LPS-primed HMDM pretreated or not with the antioxidant, *N*-acetylcysteine (NAC) (25 mM) followed by exposure for 24 h to HCS (100 μg/ml). (D) LPS-primed HMDM were exposed to the microbial toxin, nigericin (15 μM) or HCS (30 μg/ml and 100 μg/ml) for 24 h and intracellular $K^+$ levels were measured using a potassium-sensitive fluorophore, PBFI-AM (5 μM). Results in (A) to (D) are presented as mean values ± S.D. from 3 to 4 independent experiments using macrophages from different adult blood donors. $^*p < 0.05$, $^{***}p < 0.001$.

oxidative stress is a disturbance in the balance between the production of ROS and cellular antioxidant defenses [36]. Increased production of ROS has also been observed in response to a wide range of inflammasome activating agents, although it still remains unclear how ROS activate the inflammasome [19]. The source of cellular ROS is also debated. Sun et al. [37] reported that high-aspect ratio materials such as MWCNTs, but not spherical nanoparticles such as carbon black nanoparticles, induced NADPH oxidase activation in THP.1 cells, which was reduced in $p22^{phox}$-deficient cells. Moreover, the NADPH oxidase was involved in lysosomal damage, as demonstrated by decreased cathepsin B release and IL-1β production in $p22^{phox}$-deficient cells, and $p47^{phox}$-deficient mice had reduced IL-1β production and lung fibrosis in response to MWCNTs [37].

### 3.4. Hollow carbon spheres trigger IL-1β secretion in macrophages

IL-1β is an important mediator of inflammatory responses. We found a dose- and time-dependent induction of IL-1β secretion when LPS-primed macrophages were exposed to HCSs (Fig. 3a). Previous studies of particulate matter, *eg.*, silica crystals and aluminium salts, have shown that endocytosis is required for inflammasome activation leading to IL-1β production [38]. Here, we could show that pretreatment of HMDM with cytochalasin D, an inhibitor of actin polymerization, significantly reduced IL-1β production in cells exposed to HCSs (Fig. 3b).

The inflammasomes are multiprotein complexes that control the activation of caspase-1 thereby modulating the secretion of the key pro-inflammatory cytokine, IL-1β [39]. Inflammasome activation is induced by a wide range of endogenous and exogenous stimuli, such as metabolic dysregulation, microorganisms, asbestos fibers, as well as engineered nanomaterials [18]. It is still unclear how these highly varied stress signals can be detected by the inflammasome; however, the generation of ROS and the leakage of cathepsin B from lysosomes to the cytosol have been suggested to be crucial elements for the activation of inflammasome complexes [39]. In line with this, we found that HCS-induced IL-1β secretion was efficiently blocked in cells pretreated with the antioxidant, *N*-acetyl-cysteine (NAC) (Fig. 3c). Reduced intracellular $K^+$, or $K^+$ efflux, was suggested as a common trigger of inflammasome activation by bacterial toxins and particulate matter (silica, aluminum, or calcium pyrophosphate crystals) [40]. We found that exposure to

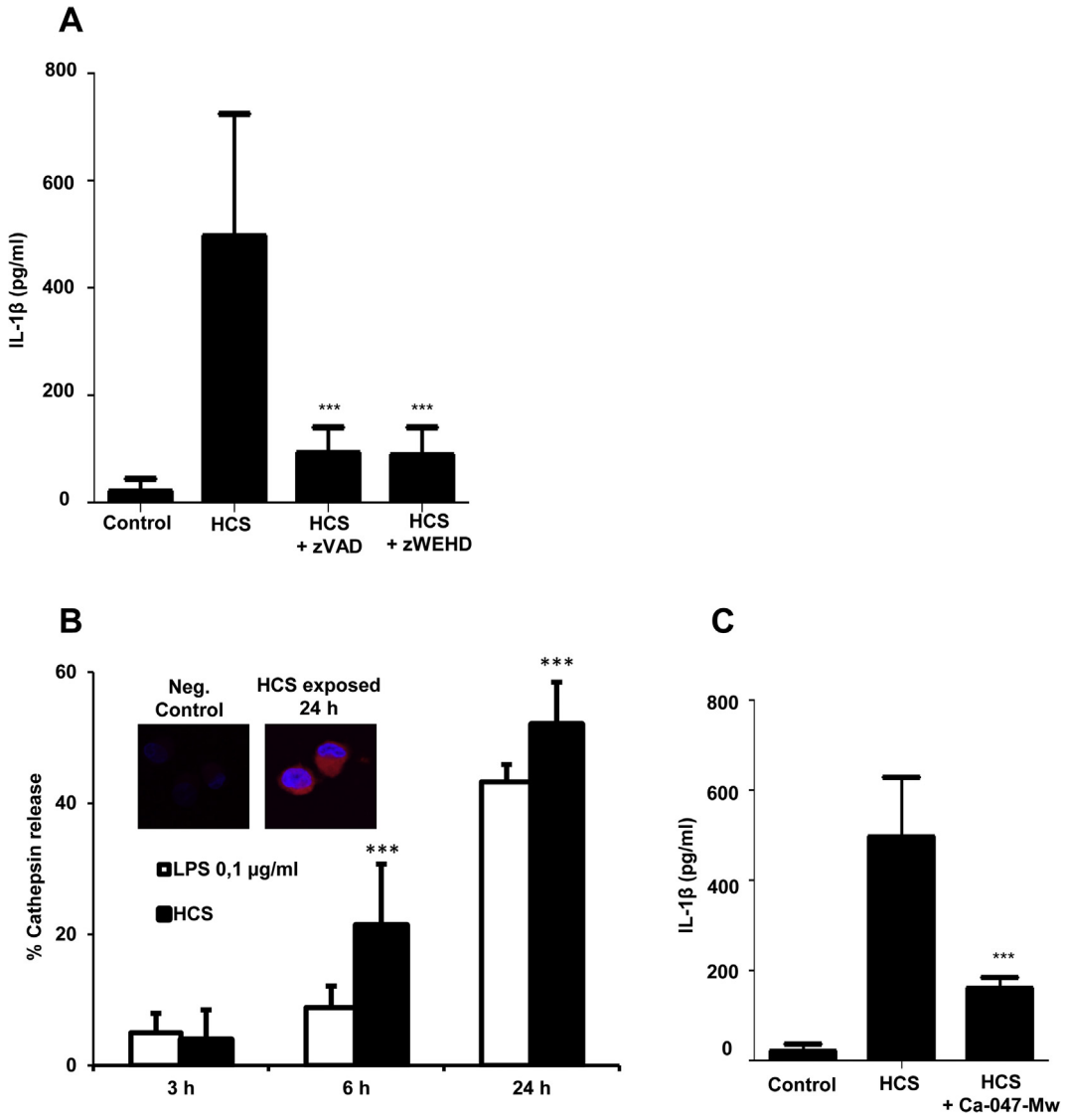


**Fig. 4.** HCS-triggered IL-1β secretion: involvement of lysosomes. (A) LPS-primed macrophages cultured for 1 h with or without the pan-caspase inhibitor, zVAD-fmk (20 μM), or the caspase-1 inhibitor, zWEHD-fmk (20 μM) were incubated with HCS (100 μg/ml) for 24 h. Cell culture supernatants were collected and IL-1β expression was assessed by ELISA. (B) LPS-primed (2 h) HMDM exposed to HCS (30 μg/ml) for the indicated time-points showed release of cathepsin B, as determined by the using Magic Red™, a cathepsin B substrate that fluoresces upon cleavage. Confocal microscopy confirmed the cytosolic distribution of cathepsin B (red), indicative of its release from lysosomes, after 24 h exposure to HCS; nuclei were counterstained using DAPI (blue) (inset). (C) IL-1β secretion in LPS-primed HMDM pretreated or not with the cathepsin B inhibitor, Ca-047-Me (10 μM) followed by exposure for 24 h to HCS (30 μg/ml). Results in (A) to (C) are shown as mean values ± S.D. from 3 to 4 independent experiments using macrophages from different healthy blood donors. ***$p < 0.001$.

HCS resulted in a reduction in intracellular $K^+$ in HMDM (Fig. 3d). The microbial toxin, nigericin was used as a positive control. Hence, our results point towards a role for endocytosis, ROS generation, and reduced intracellular $K^+$ for HCS-triggered IL-1β production.

Furthermore, we also found that IL-1β production in HMDM exposed to HCS was significantly reduced by the pan-caspase inhibitor, zVAD-fmk, and the caspase-1 inhibitor, zWEHD-fmk (Fig. 4a). To assess for lysosomal damage, we used the cathepsin B substrate, Magic Red™ [15] to study the localization of cathepsin B in HMDM exposed to HCS. As shown in Fig. 4b (inset), a diffuse cytosolic pattern was evident in exposed cells, indicative of the release of cathepsin B from lysosomes. We could also demonstrate a time-dependent cathepsin B release from lysosomes in cells exposed to HCS by spectrophotometry (Fig. 4b). In addition, pre-incubation with a cathepsin B inhibitor (Ca-047-Me) suppressed HCS-triggered secretion of IL-1β (Fig. 4c). In sum, these results suggest a role for cathepsin B as well as caspase-1 in HCS-induced IL-1β secretion, implying that HCSs elicit canonical inflammasome activation in human macrophages.

Yang et al. [17] reported recently that purified SWCNTs produced by the HiPco technique triggered IL-1β secretion in LPS-primed, bone marrow-derived dendritic cells (BMDM) from mice. The authors could show that chemical functionalization of the SWCNTs attenuated their pro-inflammatory properties, both *in vitro* and *in vivo*, in a mouse model of peritonitis [17]. For comparison, we also studied HMDMs exposed to SWCNTs (Fig. S3a). We noted a moderate, but not significant increase in cell death. ZnO nanoparticles (100 μg/ml) were used as a positive control. We observed a moderate increase in IL-1β secretion, but a statistically significant increase in cytokine production was seen only at 24 h at the highest concentration tested (100 μg/ml) (Fig. S3b). Based on these results, we conclude that HCS are more potent inducers of IL-

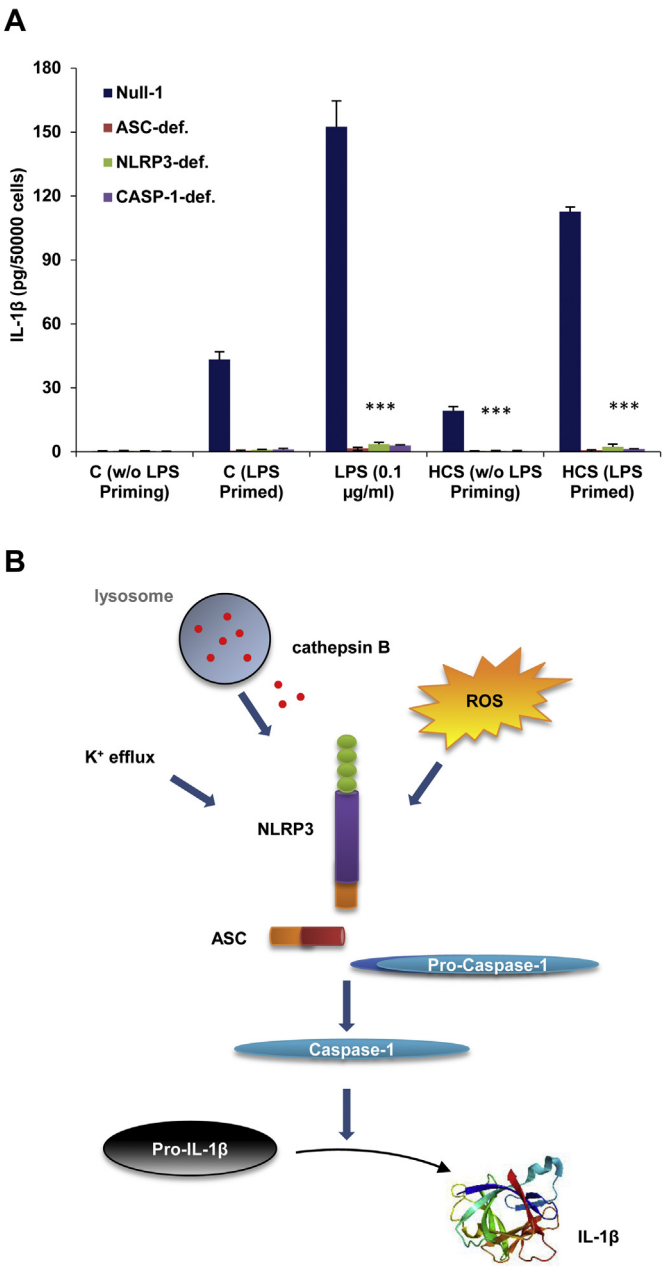


**Fig. 5.** HCS-triggered IL-1β secretion: role of NLRP3 inflammasome. (A) LPS-primed THP.1 WT cells or with knockdown of ASC (def-ACS), NLRP3 (def-NLRP3), or caspase-1 (def- CASP-1) were exposed to HCS (30 μg/ml) for 24 h and IL-1β secretion was assessed using by ELISA. Results are presented as pg/50.000 cells (mean values ± S.D.) of three independent experiments. ***$p < 0.001$. (B) Schematic view of the activation of the NLRP3 inflammasome complex.

1β secretion in HMDMs as compared to SWCNTs. In contrast, Yang et al. [17] suggested that small (5–7 nm) carbon-based nanoparticles (congealed nanodiamonds) were less potent inducers of IL-1β production in BMDM than SWCNTs. In an earlier study, Reisetter et al. [13] demonstrated that carbon black nanoparticles (20 nm) triggered caspase-1-mediated pyroptosis with IL-1β secretion in primary human alveolar macrophages. These differences could be related to differences in particle properties or differences in the cell model used; in addition, the presence of endotoxin contamination should be ruled out when immune cells are used.

### 3.5. Hollow carbon spheres trigger NLRP3 inflammasome activation

To date, five proteins have been confirmed to assemble inflammasomes, including the nucleotide-binding oligomerization domain (NOD), leucine-rich repeat (LRR)-containing protein (NLR) family members NLRP1, NLRP3 and NLRC4, as well as AIM2 and pyrin (see Ref. [39] for a recent review). NLRP3 (also known as NALP3) responds to a broad range of different stimuli, including non-microbial factors such as silica, asbestos, and nanomaterials, *eg.*, MWCNTs. Recognition of the ligand results in the recruitment of an adaptor protein known as ASC, which consists of two domains: a pyrin domain (PYD) and a caspase recruitment domain (CARD). These domains allow ASC to connect the inflammasome sensor molecule to pro-caspase-1. Proximity-induced autoprocessing then results in the formation of catalytically active caspase 1, which processes pro-IL-1β leading to the release of IL-1β [39] (and see Fig. 5b).

To determine whether HCSs elicit NLRP3 inflammasome activation, we used the human monocyte-like cell line, THP.1 with stable knockdown of ASC (def-ACS), NLRP3 (def-NLRP3), or caspase-1 (def- CASP-1). The wild-type (WT) THP.1 cell line was used for reference. Following LPS priming, HCS triggered IL-1β secretion in THP.1 WT cells, but not in def-NLRP3, def-ACS, or def-CASP-1 cells, thus demonstrating a role of the NLRP3 inflammasome (Fig. 5a). Fig. 5b provides a schematic view of NLRP3 inflammasome activation.

## 4. Conclusions

HCS have received considerable attention for their potential use in energy storage devices. However, there are few if any studies on the potential hazard of these carbon-based nanoparticles. The present study has provided evidence of inflammasome-dependent secretion of pro-inflammatory IL-1β release in primary human macrophages exposed to HCS. However, no cytotoxicity (loss of cell viability) was noted. A previous studies suggested that diverse inflammasome activating agents triggered IL-1β secretion by triggering necrosis [41]. However, our results using HCS do not support this model of “cell rupture-associated” IL-1β release. The latter study was performed using human or murine cell lines, and results were not validated using primary macrophages. In a very recent study, it was demonstrated at the single cell level that IL-1β can be released from live, metabolically active cells following caspase-1 activation [42]. The present findings indicate that cell death and inflammasome activation induced by nanomaterials may transpire as independent processes, and we suggest, therefore, that both phenomena, *i.e.*, cytotoxicity/cell death and inflammasome-driven cytokine secretion should be evaluated independently for each novel nanomaterial, to determine the hazard potential.

## Competing interest

The authors declare that they have no competing financial interests.

## Disclaimer

The findings and conclusions herein are those of the authors and do not necessarily represent the views of the National Institute for Occupational Safety and Health of the United States.

## Acknowledgements

This work was supported by the European Commission (FP7-NANOMMUNE, No. 214281; FP7-MARINA, No. 263215; Flagship

Project GRAPHENE, No. 604391, and No. 696656), the Swedish Research Council for Environment, Agricultural Sciences and Spatial Planning, National Institute for Occupational Safety and Health (Grant No. 939011k), and the University of Cologne, Cologne, Germany. F.T.A. was supported, in part, through a postdoctoral fellowship from the Galician Government, Spain. Dr. Xuefeng Song, University of Cologne, is acknowledged for assistance in the preparation of hollow carbon spheres.

## Appendix A. Supplementary data

Supplementary data related to this article can be found at http://dx.doi.org/10.1016/j.carbon.2016.11.049.

## References

[1] V.C. Sanchez, A. Jachak, R.H. Hurt, A.B. Kane, Biological interactions of graphene-family nanomaterials: an interdisciplinary review, Chem. Res. Toxicol. 25 (2012) 15–34.
[2] K. Bhattacharya, S.P. Mukherjee, A. Gallud, S.C. Burkert, S. Bistarelli, S. Bellucci, M. Bottini, A. Star, B. Fadeel, Biological interactions of carbon-based nanomaterials: from coronation to degradation, Nanomedicine 12 (2016) 333–351.
[3] K. Bhattacharya, F.T. Andón, R. El-Sayed, B. Fadeel, Mechanisms of carbon nanotube-induced toxicity: focus on pulmonary inflammation, Adv. Drug Deliv. Rev. 65 (2013) 2087–2097.
[4] S. Yang, X. Feng, L. Zhi, Q. Cao, J. Maier, K. Müllen, Nanographene-constructed hollow carbon spheres and their favorable electroactivity with respect to lithium storage, Adv. Mater. 22 (2010) 838–842.
[5] Z.-C. Yang, Y. Zhang, J.-H. Kong, S.Y. Wong, X. Li, J. Wang, Hollow carbon nanoparticles of tunable size and wall thickness by hydrothermal treatment of α-cyclodextrin templated by F127 block copolymers, Chem. Mater. 25 (2013) 704–710.
[6] X. Li, L. Zhang, G. He, $Fe_3O_4$ doped double-shelled hollow carbon spheres with hierarchical pore network for durable high-performance supercapacitor, Carbon 99 (2016) 514–522.
[7] F.T. Andón, B. Fadeel, Programmed cell death: molecular mechanisms and implications for safety assessment of nanomaterials, Acc. Chem. Res. 46 (2012) 733–742.
[8] L. Zhu, D.W. Chang, L. Dai, Y. Hong, DNA damage induced by multiwalled carbon nanotubes in mouse embryonic stem cells, Nano Lett. 7 (2007) 3592–3597.
[9] Y. Zhang, S.F. Ali, E. Dervishi, Y. Xu, Z. Li, D. Casciano, A.S. Biris, Cytotoxicity effects of graphene and single-wall carbon nanotubes in neural phaeochromocytoma-derived pc12 cells, ACS Nano 4 (2010) 3181–3186.
[10] A. Sasidharan, L.S. Panchakarla, P. Chandran, D. Menon, S. Nair, C.N.R. Rao, et al., Differential nano-bio interactions and toxicity effects of pristine versus functionalized graphene, Nanoscale 3 (2011) 2461–2464.
[11] G. Qu, S. Liu, S. Zhang, L. Wang, X. Wang, B. Sun, et al., Graphene oxide induces Toll-like receptor 4 (TLR4)-dependent necrosis in macrophages, ACS Nano 7 (2013) 5732–5745.
[12] J. Palomäki, J. Sund, M. Vippola, P. Kinaret, D. Greco, K. Savolainen, et al., A secretomics analysis reveals major differences in the macrophage responses towards different types of carbon nanotubes, Nanotoxicology 9 (2015) 719–728.
[13] A.C. Reisetter, L.V. Stebounova, J. Baltrusaitis, L. Powers, A. Gupta, V.H. Grassian, et al., Induction of inflammasome dependent pyroptosis by carbon black nanoparticles, J. Biol. Chem. 286 (2011) 21844–21852.
[14] J. Palomäki, E. Välimäki, J. Sund, M. Vippola, P.A. Clausen, K.A. Jensen, et al., Long, needle-like carbon nanotubes and asbestos activate the NLRP3 inflammasome through a similar mechanism, ACS Nano 5 (2011) 6861–6870.
[15] R. Li, X. Wang, Z. Ji, B. Sun, H. Zhang, C.H. Chang, et al., Surface charge and cellular processing of covalently functionalized multiwall carbon nanotubes determine pulmonary toxicity, ACS Nano 7 (2013) 2352–2368.
[16] S. Hussain, S. Sangtian, S.M. Anderson, R.J. Snyder, J.D. Marshburn, A.B. Rice, et al., Inflammasome activation in airway epithelial cells after multi-walled carbon nanotube exposure mediates a profibrotic response in lung fibroblasts, Part Fibre Toxicol. 11 (2014) 28.
[17] M. Yang, K. Flavin, I. Kopf, G. Radics, C.H. Hearnden, G.J. McManus, et al., Functionalization of carbon nanoparticles modulates inflammatory cell recruitment and NLRP3 inflammasome activation, Small 9 (2013) 4194–4206.
[18] B. Sun, X. Wang, Z. Ji, R. Li, T. Xia, NLRP3 inflammasome activation induced by engineered nanomaterials, Small 9 (2013) 1595–1607.
[19] V. Rabolli, D. Lison, F. Huaux, The complex cascade of cellular events governing inflammasome activation and IL-1β processing in response to inhaled particles, Part Fibre Toxicol. 13 (2016) 40.
[20] J. Shi, H.L. Karlsson, K. Johansson, V. Gogvadze, L. Xiao, J. Li, et al., Microsomal glutathione transferase 1 protects against toxicity induced by silica nanoparticles but not by zinc oxide nanoparticles, ACS Nano 6 (2012) 1925–1938.
[21] A. Kapralov, W.H. Feng, A. Amoscato, N. Yanamala, K. Balasubramanian, D.E. Winnica, et al., Adsorption of surfactant lipids by single-walled carbon nanotubes in mouse lung upon pharyngeal aspiration, ACS Nano 6 (2012) 4147–4156.
[22] X.R. Xia, N. Monteiro-Riviere, S. Mathur, X. Song, L. Xiao, S.J. Oldenberg, et al., Mapping the surface adsorption forces of nanomaterials in biological systems, ACS Nano 5 (2011) 9074–9081.
[23] W. Stöber, A. Fink, E. Bohn, Controlled growth of monodisperse silica spheres in the micron size range, J. Colloid Interface Sci. 26 (1968) 62–69.
[24] N. Feliu, M.V. Walter, M.I. Montañez, A. Kunzmann, A. Hult, A. Nyström, et al., Stability and biocompatibility of a library of polyester dendrimers in comparison to polyamidoamine dendrimers, Biomaterials 33 (2012) 1970–1981.
[25] A. Naji, B.A. Muzembo, K. Yagyu, N. Baba, F. Deschaseaux, L. Sensebé, et al., Endocytosis of indium-tin-oxide nanoparticles by macrophages provokes pyroptosis requiring NLRP3-ASC-Caspase1 axis that can be prevented by mesenchymal stem cells, Sci. Rep. 6 (2016) 26162.
[26] X. Sun, Y. Li, Colloidal carbon spheres and their core/shell structures with noble-metal nanoparticles, Angew. Chem. Int. Ed. Engl. 43 (2004) 597–601.
[27] S. Ding, J.S. Chen, G. Qi, X. Duan, Z. Wang, E.P. Giannelis, et al., Formation of $SnO_2$ hollow nanospheres inside mesoporous silica nanoreactors, J. Am. Chem. Soc. 133 (2011) 21–23.
[28] X. Lai, J. Li, B.A. Korgel, Z. Dong, Z. Li, F. Su, et al., General synthesis and gas-sensing properties of multiple-shell metal oxide hollow microspheres, Angew. Chem. Int. Ed. Engl. 50 (2011) 2738–2741.
[29] S.L. Cassel, S.C. Eisenbarth, S.S. Iyer, J.J. Sadler, O.R. Colegio, L.A. Tephly, et al., The Nalp3 inflammasome is essential for the development of silicosis, Proc. Natl. Acad. Sci. U. S. A. 105 (2008) 9035–9040.
[30] A.S. Yazdi, G. Guarda, N. Riteau, S.K. Drexler, A. Tardivel, I. Couillin, et al., Nanoparticles activate the NLR pyrin domain containing 3 (Nlrp3) inflammasome and cause pulmonary inflammation through release of IL-1α and IL-1β, Proc. Natl. Acad. Sci. U. S. A. 107 (2010) 19449–19454.
[31] Y.S. Lee, Syntheses and properties of fluorinated carbon materials, J. Fluor. Chem. 128 (2007) 392–403.
[32] G.J. Oostingh, E. Casals, P. Italiani, R. Colognato, R. Stritzinger, J. Ponti, et al., Problems and challenges in the development and validation of human cell-based assays to determine nanoparticle-induced immunomodulatory effects, Part Fibre Toxicol. 8 (2011) 8.
[33] H. Vallhov, J. Qin, S.M. Johansson, N. Ahlborg, M.A. Muhammed, A. Scheynius, et al., The importance of an endotoxin-free environment during the production of nanoparticles used in medical applications, Nano Lett. 6 (2006) 1682–1686.
[34] R. Hamid, Y. Rotshteyn, L. Rabadi, R. Parikh, P. Bullock, Comparison of alamar blue and MTT assays for high through-put screening, Toxicol In Vitro 18 (2004) 703–710.
[35] N.A. Monteiro-Riviere, A.O. Inman, L.W. Zhang, Limitations and relative utility of screening assays to assess engineered nanoparticle toxicity in a human cell line, Toxicol. Appl. Pharmacol. 234 (2009) 222–235.
[36] A.A. Shvedova, A. Pietroiusti, B. Fadeel, V.E. Kagan, Mechanisms of carbon nanotube-induced toxicity: focus on oxidative stress, Toxicol. Appl. Pharmacol. 261 (2012) 121–133.
[37] B. Sun, X. Wang, Z. Ji, M. Wang, Y.P. Liao, C.H. Chang, et al., NADPH oxidase-dependent NLRP3 inflammasome activation and its important role in lung fibrosis by multiwalled carbon nanotubes, Small 11 (2015) 2087–2097.
[38] V. Hornung, F. Bauernfeind, A. Halle, E.O. Samstad, H. Kono, K.L. Rock, et al., Silica crystals and aluminum salts activate the NALP3 inflammasome through phagosomal destabilization, Nat. Immunol. 9 (2008) 847–856.
[39] P. Broz, V.M. Dixit, Inflammasomes: mechanism of assembly, regulation and signalling, Nat. Rev. Immunol. 16 (2016) 407–420.
[40] R. Muñoz-Planillo, P. Kuffa, G. Martínez-Colón, B.L. Smith, T.M. Rajendiran, G. Núñez, $K^+$ efflux is the common trigger of NLRP3 inflammasome activation by bacterial toxins and particulate matter, Immunity 38 (2013) 1142–1153.
[41] S.P. Cullen, C.J. Kearney, D.M. Clancy, S.J. Martin, Diverse activators of the NLRP3 inflammasome promote IL-1β secretion by triggering necrosis, Cell Rep. 11 (2015) 1535–1548.
[42] S.A. Conos, K.E. Lawlor, D.L. Vaux, J.E. Vince, L.M. Lindqvist, Cell death is not essential for caspase-1-mediated interleukin-1β activation and secretion, Cell Death Differ. 23 (2016) 1827–1838.